Pergamon

Cement and Concrete Research, Vol. 27, No. 7, pp. 1047-1060, 1997

0008-8846/97 $17.00 + .00

PII S0008-8846(97)00094-X

# AN EVALUATION OF CONTROLLED PERMEABILITY FORMWORK FOR LONG-TERM DURABILITY OF STRUCTURAL CONCRETE ELEMENTS

**A.K. Suryavanshi and R.N. Swamy**
Department of Mechanical Engineering, University of Sheffield, Sheffield, UK, S1 4DU

(Refereed)
(Received April 3, 1996; in final form May 12, 1997)

## ABSTRACT

The long-term performance of a concrete slab (CPF slab) exposed to chloride ingress and atmospheric carbonation from the surface generated by controlled permeability formwork (CPF) is investigated. The results are compared with a similar slab exposed to long-term chloride ingress and atmospheric carbonation from the cast face (Control slab). Techniques such as X-ray diffraction (XRD) and differential thermal analyses (DTA) were employed to determine the resistance against carbonation while, mercury porosimetry was used for investigating the pore size distribution at the surface of the slabs. Amount of acid soluble chlorides was determined by using Volhard's method.

The CPF employed at the bottom of the mould was not fully effective in its intended purpose of generating a permanent and dense impermeable concrete layer adjacent to it when the design water-cement (w/c) ratio of the concrete mix was 0.60. This resulted in an almost similar extent of carbonation at the surface for both CPF and control slabs as shown by XRD and DTA studies. Similarly, there were no significant differences in the amount of chlorides and their depths of penetration for both CPF and control slabs, although the former was marginally superior in chloride penetration resistance at the surface. © *1997 Elsevier Science Ltd*

## Introduction

For attaining long-term durability and protecting the reinforcement steel from corrosion, an impermeable concrete cover is essential for structural elements. Conventionally, this is achieved by increasing the cement content for the entire volume of concrete used in the structure, although the requirement is critical only in the cover region. However, increasing the cement content for the entire volume of concrete leads to increased cost. Thus, alternative methods have been attempted to improve the quality of the exposed outer layer of concrete, without increasing the cement content for the entire structure.

Recent research in Japan has led to the development of an unique type of permeable formwork as a replacement to the conventional impermeable formwork (1-3). The permeable formwork is known to generate a dense concrete at the surface in contact with it (1-5). In literature, this special kind of formwork is often called "Controlled Permeability Formwork (CPF)". The principle underlying the CPF is that, the formwork acts as a filter through which

the entrapped air and the surplus water are drained off on placing and vibrating the concrete. The technique essentially consists of lining the inner surface of the pre-drilled formwork with a custom designed fabric material before placing the concrete. The very essential requirement of the fabric material is its ability to filter air and water effectively while minimizing the loss of cement. The methods for determining the water and air permeability of the fabric material are covered in ASTM standards 4491-85 and 737-75 respectively (6,7).

The concrete surface layer thus generated in contact with the CPF is reported to be highly impermeable with a water-cement (w/c) ratio as low as 0.3, for a concrete mixed at a w/c ratio of 0.5-0.55 (8). Laboratory based short-term study on a C30 grade concrete cast with the CPF showed a 50% reduction in chloride diffusion coefficient compared to the conventionally cast concrete of similar grade (5). The concrete cast with CPF was also effective in reducing the depths of carbonation for both high and low strength concrete. For high strength concrete such as C50, over a period of 11 months of exposure to laboratory environment, the reduction in depth of carbonation was almost 50%, compared to the concrete cast without the CPF under similar conditions (5). Thus, on short-term exposure, the CPF enhanced the durability of concrete against atmospheric carbonation attack and chloride penetration. Furthermore, the CPF significantly increased the surface hardness, and improved the surface texture with minimum surface defects such as blowholes even in high strength concrete such as C50 (5). The blowholes on the surface are critical in structures such as the dam spillways, as these can act as nuclei for cavitation damage. However, all the above improvements in properties of concrete are confined to a depth of 10-30 mm from the surface in contact with the CPF (1-5,8). The CPF is also used to reduce the form-pressure during casting as draining off the entrapped air and the surplus water from interface relieves the pressure.

Investigations on the durability aspects of concrete cast with the CPF are limited in literature. Further, the investigators have used more conventional techniques such as Schmidt hammer test, water and oxygen permeability measurements, water sorptivity tests and phenolphthalein spray tests (for carbonation depths) to evaluate the performance of concrete cast in contact with the CPF.

In the present investigation, an attempt is made to understand in depth the durability of concrete cast in contact with the CPF on a long-term basis against atmospheric carbonation and chloride penetration. Techniques such as XRD, DTA, mercury porosimetry and Volhard's method for acid soluble chlorides have been used as experimental techniques.

## Experimental Work

1. Test Specimen Preparation and Exposing to Test Condition. In the present experimental investigation instead of using a number of small specimens, two slabs (500 × 500 × 150 mm) of fairly large surface area (2500 sq. cm) were prepared. Further, a number of samples were drawn randomly covering the entire exposed surface of the slabs to generate an average result.

Both the above slabs were cast using the CPF at the bottom of the mould. Before placing the concrete, the permeable fabric was stretched in perpendicular directions and was then fixed and tightened on to the bottom mould. The bottom mould had pre-drilled holes to drain off the surplus water and also the entrapped air after placing the concrete. A polypropylene fabric, "Zemdrain Membrane" was used in the present investigation. According to the only cementitious material in the mix. The cement content in the concrete mix was fixed at 350 kg $m^{-3}$ and the aggregate/cement ratio was kept at 5.26. A special method of concrete mixing

as described below was adopted to obtain an uniform mix with minimum bleeding during setting. To start with, all the coarse aggregates along with 1/3rd of the total mixing water were added to the mixer, and they were mixed for 30 seconds. The fine aggregates and the cement were then added to the mix, and these were mixed for 30 seconds. Finally, the remaining mixing water was added, and the mixing was continued for another 90 seconds.

The mixed concrete was then poured in three different layers in the mould, and each layer was vibrated with a poker vibrator until no more air bubbles were seen emerging. After casting, the slabs were covered with polyethylene sheet for 24 hours. Then the slabs were subjected to wet curing by ponding water on the top surface for 6 days, and afterwards the slabs were sponge dried, demoulded, and finally, the fabric was separated from the slab. One of the slabs was now inverted so that the surface generated by the CPF was at the top, while for the other slab, the cast face remained at the top. The slabs were then exposed to ambient conditions for 21 days for further air curing. In the following section, the slab which was inverted so as to bring the CPF generated face at the top will be called the "CPF slab" while, the other slab with cast face on top is termed the "control slab". It is reported in literature that the CPF is effective in generating a relatively dense concrete upto a maximum depth of 10-30 mm from the CPF mould (1-5,8). Hence, for the control slab, placing the CPF at the bottom mould would not influence the permeation characteristics of the concrete near the cast face.

To facilitate chloride solution ponding on the slabs, an acrylic frame of 50 mm in height and exactly fitting along the outer edges of the slab was glued at the top of each slab. This frame at the top served as an embankment for ponding of the salt solution. The slabs were then exposed to cyclic ponding with 4% sodium chloride (NaCl) solution at the top surface followed by drying. Each cycle consisted of ponding for 7 days, then removal of the solution, and drying the surface at ambient condition for 3 days. Freshly prepared solution was used for each cycle, and the depth of ponding was kept constant at 10 mm. The ponding from the top surface of slabs was continued for a total of 70 cycles in steps of 10, 20, 50 and 70 cycles. Short time gaps in terms of days were maintained between 10 and 20, and between 20 and 50 cycles. Longer time gap of about one and half years was deliberately maintained between 50 and 70 cycles. After completing 70 cycles of ponding and drying, the slabs were exposed to a laboratory drying environment for about two and half years similar to that of an interior of a building.

2. Chloride Penetration and Carbonation Studies. After completing 70 exposure cycles followed by the two and half years' exposure to laboratory environment, the slabs were subjected to a variety of experimental investigations. The first stage of the experimental investigation consisted in establishing an acid soluble chloride profile over the depth of the slabs. During this first stage, the degree of atmospheric carbonation at the surface of the slabs was also investigated.

For establishing the acid soluble chloride profile over the depth of the slabs, the slabs were cored with a water lubricated vacuum based Hilti core cutter. The slabs were cored using a 25 mm diameter core cutter at four randomly selected locations to a depth varying between 105 and 115 mm from the top exposed surface. The cores were then sliced using a water lubricated circular saw into following depths: 0-5, 5-25, 25-45, 45-65, 65-85 and 85-105 mm. The sliced samples were then passed twice through a jaw crusher. In order to get a representative sample for each slab at a given depth, the sliced samples from the same depth were mixed. To separate the large aggregates, the coarsely crushed samples were then passed through a 2 mm sieve. The coarsely crushed particles were finally crushed to a fine size by

crushing them in a heavy duty pestle mortar. Finally, the crushed samples from the pestle mortar were passed through a 150 μm sieve and the powder was used for acid soluble chloride analyses. The acid soluble chloride contents by weight of cement were determined indirectly by Volhard's method as described in BS 1881 (9).

To study the extent of carbonation at the exposed surface of the slabs, techniques such as powder method of XRD and DTA were used. The powder samples left over from the chloride analyses were used for the above studies.

The XRD studies were carried out on a Phillips X-ray diffractometer with a X-ray source of Cu $K_\alpha$ radiation ($\lambda$ = 1.5418 A°). The scan speed was 2° per minute with scan step of 0.02°. The X-ray tube current and voltage were fixed at 30 mA and 50 KV respectively for all the samples. The "front loading" method was adopted for loading the sample into the aluminium window.

A Stanton Redcroft DTA (model 673-4) was used for thermal studies. Powdered samples weighing 100 mg were used in order to make the samples more representative, although this might result in thermal gradients within the sample. The samples were scanned from room temperature to 850°C with a scan speed of 10°C per minute. Platinum crucibles were used for filling both the sample and the reference material (alumina ignited to 1100°C).

3. Pore Size Distribution Studies. The second stage of the experimental work deals with the study of pore size distribution at the ponded surfaces of slabs. For this study, the slabs were once again cored with a 25 mm diameter core cutter to a depth of 30 mm from top ponded surface as already explained. The cores were then sliced as previously explained into the following depths: 0-5 mm and 5-25 mm. The cored slices were then reduced to small mortar fragments using a light weight hammer and a small chisel separating the coarse aggregates. It is believed that this method of sample preparation results in a minimum damage to the pore structure of the sample. The size of the chiselled irregular mortar samples was slightly larger than the maximum coarse aggregate size (10 mm). These mortar samples were then soaked in methanol (solvent extraction) in air tight polypropylene bottles for a minimum period of 10-15 days. The samples were then dried in an oven held at a temperature of 105°C until the samples reached a constant weight. The heating time for reaching a constant weight did not normally exceed 2-3 hours as the samples were small in size. Upon reaching a constant weight, the samples were removed from the oven and were stored in a desiccator until the day of the experiment. The above method of drying the sample is known to preserve the original pore structure of the sample (10).

The pore size distribution study was carried out on a Micromeritics Pore Sizer (Model 9320) having a high pressure limit of 30,000 psia. The contact angle "θ" used in the Washburn equation was 117° as the sample was oven dried followed by solvent extraction (11). The pores were assumed to be of circular cross section and hence, the shape factor "ϕ" in the Washburn equation was chosen as 4. Weight of the samples used for the pore structure studies varied between 2 and 2.5 grams.

## Results

In the following section the results of the tests carried on the samples drawn from CPF slab are compared with those from the control slab.

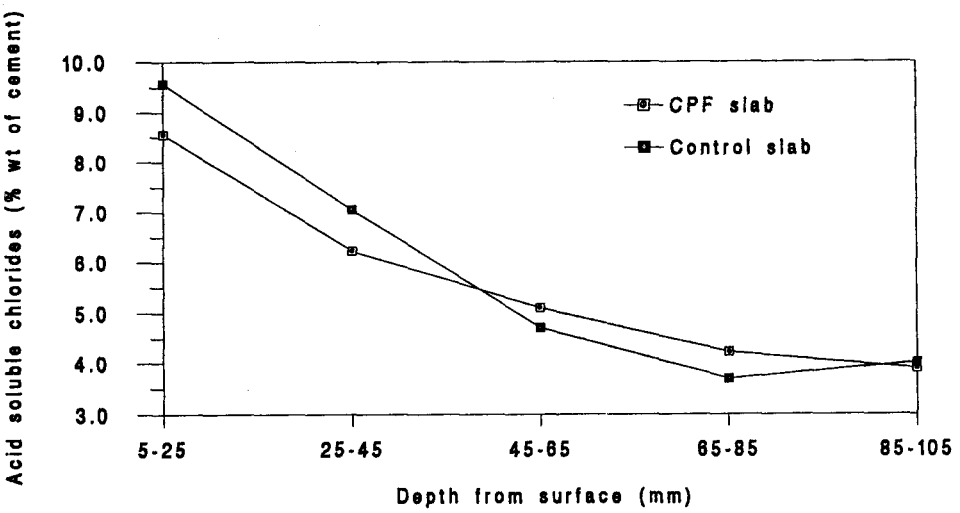


FIG. 1.
Acid soluble chloride contents for the CPF and control slabs.

1. Chloride Analysis. Figure 1 shows the chloride contents at different depth intervals for the CPF slab and the control slab for which ponding with NaCl solution was done from the cast face. The results presented in the above figure are after ponding the surface of the slabs for 70 cycles of wetting and drying.

In general, both slabs show almost identical chloride contents at any given depth, with chloride contents decreasing with increasing distance from the surface. Compared to the control slab, the CPF slab shows relatively lower acid soluble chlorides at the top; however, beyond the 25-45 mm depth interval, the CPF slab shows relatively higher amount of acid soluble chlorides. Thus, the CPF slab is marginally superior in chloride penetration resistance than the control slab until the 25-45 mm depth interval. The results obtained after 10, 30 and 50 cycles of wetting and drying, though not presented here, also support the above view (12).

Acid soluble chloride contents for the 0-5 mm depth interval were not analyzed as abnormally high build-up of chlorides at the surface is expected. This is primarily because of the chloride precipitation at the surface during the drying periods.

2. XRD and DTA Results. All the XRD diffractograms presented below are plotted with an identical scale for the y-axis; that is, the number of counts, and hence they are comparable. Similarly, all the DTA thermograms presented below are also plotted with an identical scale for the y-axis; namely, the temperature differences ($\Delta T$).

*2.1. Slab ponded from the surface generated by the CPF (CPF slab).* Figure 2 presents the X-ray diffractograms for 0-5 mm and 5-25 mm depth intervals from the top ponded surface. The diffractogram for the 0-5 mm shows a relatively large maximum intensity peak for calcite ($CaCO_3$) at 3.04 A° compared to that for the 5-25 mm depth interval. The meta-stable vaterite ($CaCO_3$) is also evident at 2.06 A° for the 0-5 mm depth interval. Portlandite is evident for both the above depth intervals through a maximum intensity peak at 2.63 A°. The presence of calcite and vaterite is explained by the chemical conversion of a part of free portlandite to $CaCO_3$ (calcite and vaterite) in the presence of moisture and atmospheric

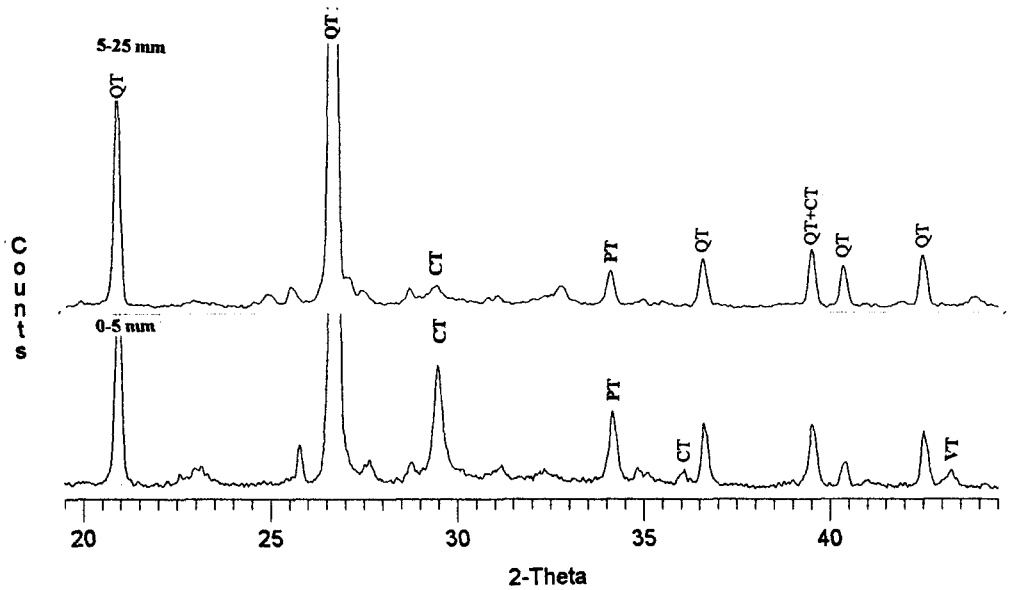


FIG. 2.
XRD diffractograms for the CPF slab. (Keys: QT: α-Quartz, PT: Protlandite, CT: Clacite and VT: Vaterite. The keys in bold letters indicate the maximum intensity peaks).

carbon dioxide ($CO_2$). From Figure 2 it appears that, the 0-5 mm depth interval has greater proportion of portlandite than the 5-25 mm depth interval despite the fact that the former was carbonated to a greater extent.

The above XRD results are inconclusive as other hydrated cement phases having identical d-spacing are some times mistakenly identified. For example, the poorly crystalline C-S-H gel is known to give a broad and weak peak around 3.07 A° close enough to calcite (13). The peak intensity for a phase like portlandite from X-ray diffractogram is sometimes unreliable due to the preferred orientation exhibited by portlandite crystals, although this can be minimised by "back loading" the aluminium window (14). Furthermore, due to the presence of calcite in both crystalline and amorphous forms in hydrated cement, the results from XRD are inconclusive in identifying the total quantity of calcite formed in concrete (15,16). This is because the XRD identifies only those phases existing in well-crystalline form. Thermal studies such as DTA, or differential scanning calorimetry (DSC) are useful for identifying amorphous and crystalline calcite present in concrete. On a DTA thermogram, the decomposition of crystalline calcite is indicated through an endothermic peak centered close to 800°C, while the amorphous calcite decomposes at relatively lower temperatures than the well-crystalline calcite (15,16). The higher degree of dispersity (lower activation energy) associated with the amorphous calcite is believed to lower its decomposition temperature (16).

Similarly, portlandite on a DTA thermogram starts dehydrating to CaO at about 400°C, and therefore gives rise to a strong endothermic peak around 500°C (17). The α-quartz gives an endothermic peak at 573°C at which it transforms into β-quartz (13).

Figure 3 shows the DTA thermograms for 0-5 mm and 5-25 mm depth intervals. The thermograms for the 0-5 mm depth interval shows endothermic peaks centered at 805°C and 765°C to indicate the presence of calcite in well-crystalline (as shown by XRD) and

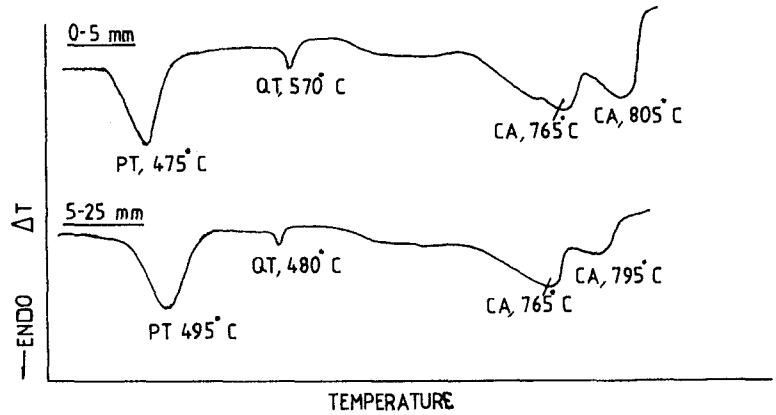


FIG. 3.
DTA thermograms for the CPF slab. (Keys: PT: Portlandite, CA: Calcite, QT: α-Quartz).

amorphous forms respectively. Similarly, the 5-25 mm depth interval also shows two endothermic peaks centered at 795°C and 765°C to indicate the presence of well-crystalline (as shown by XRD) and amorphous calcite respectively. By taking the total peak height due to both crystalline and amorphous calcite as a criterion for estimating the extent of carbonation attack, it appears that the 0-5 mm depth interval is carbonated to a greater extent than the 5-25 mm depth interval. Both 0-5 and 5-25 mm depth intervals also indicate the presence of portlandite through endothermic peaks centered at 475°C and 495°C respectively. By comparing the peak heights for portlandite, it is evident that the 0-5 mm has a slightly greater amount of portlandite than the 5-25 mm depth interval despite the former was carbonated to a higher extent. The XRD results presented in Figure 2 also support the above observation.

*2.2. Slab ponded from the cast face (control slab).* Figure 4 presents the XRD diffractograms for 0-5 mm and 5-25 mm depth intervals. The diffractogram for the 0-5 mm depth interval shows a relatively large maximum intensity peak for calcite at 3.04 A° compared to the diffractogram for the 5-25 mm depth interval. The 0-5 mm depth interval, apart from calcite also shows a maximum intensity peak for vaterite at 2.06 A°, which is absent in the diffractogram for the 5-25 mm depth interval. The above evidence indicates the relatively higher extent of carbonation of the slab at the 0-5 mm depth interval. The above observation is also supported by the total absence of portlandite for the 0-5 mm depth interval. On the other hand, portlandite is evident for the 5-25 mm depth interval indicating relatively lower extent of carbonation at the 5-25 mm depth interval.

Figure 5 presents the DTA thermograms for 0-5 mm and 5-25 mm depth intervals. The thermogram for the 0-5 mm depth interval shows a large endothermic peak centered at 790°C to indicate the presence of crystalline calcite (as shown by XRD results). On the other hand, the thermogram for the 5-25 mm depth interval shows relatively smaller endothermic peaks centered at 785°C and 735°C to indicate the presence of well-crystalline (as shown by XRD results) and amorphous calcite respectively. In conformity with the XRD results, the thermogram for the 0-5 mm depth interval also shows the absence of portlandite. In contrast, the thermogram for the 5-25 mm depth interval shows an endothermic peak centered at 510°C to indicate the presence of portlandite.

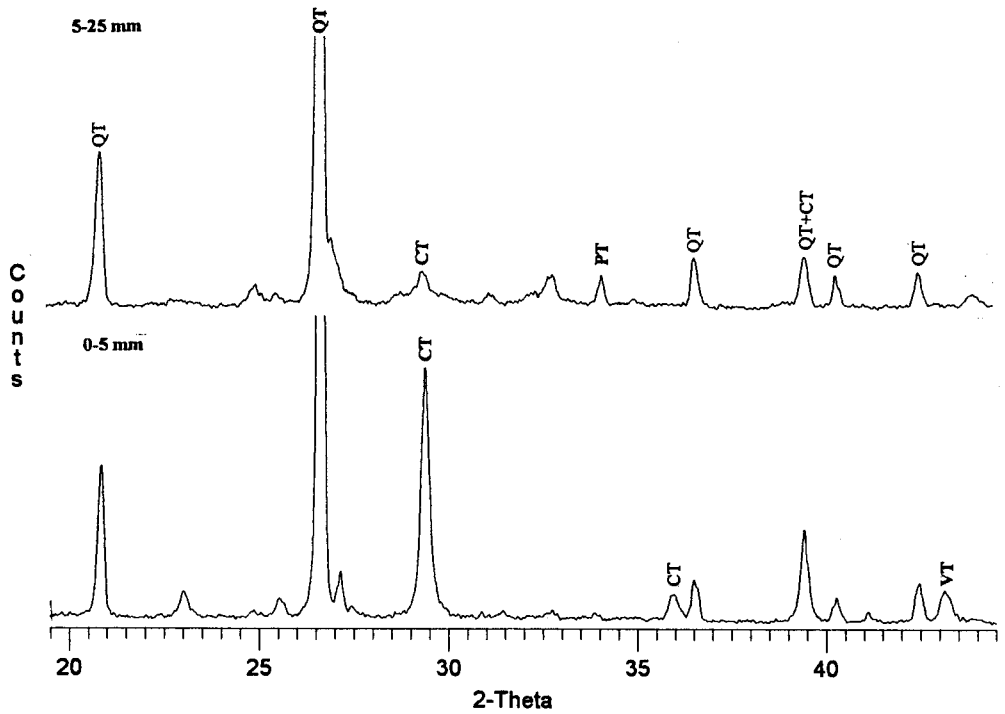


FIG. 4.
XRD diffractograms for the control slab. (Keys: QT: α-Quartz, PT: Portlandite, CT: Calcite and VT: Vaterite. The keys in bold letters indicate the maximum intensity peaks).

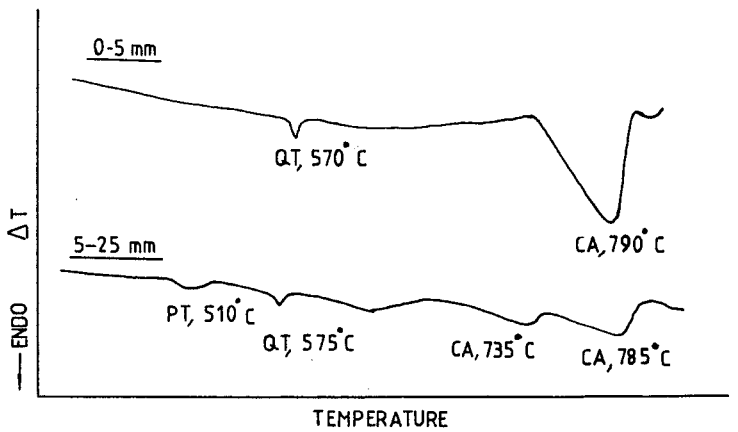


FIG. 5.
DTA thermograms for the slab ponded from the cast face. (Keys: PT: Portlandite, CA: Calcite, QT: α-Quartz).

By inter comparison of the DTA thermograms presented in Figures 3 (CPF slab) and 5 (control slab) the following observations are evident. By taking the total peak height due to both well-crystalline and amorphous calcite as a criterion, the 0-5 mm depth interval of both CPF and control slabs appears to have carbonated to a nearly similar extent. Despite the similar extent of carbonation at the 0-5 mm depth interval, the CPF slab shows the presence of significant amount of portlandite at the 0-5 mm depth interval while, portlandite was absent for the control slab at the above depth interval. Similarly, the 5-25 mm depth interval of both CPF and control slabs also appears to have carbonated to a nearly similar extent. However, the CPF slab shows a greater amount of portlandite than the control slab at the 5-25 mm depth interval. The other important observation was the presence of slightly greater amount of portlandite at the 0-5 mm than the 5-25 mm depth interval of the CPF slab despite the fact that the former was carbonated to a greater extent (Figures 2 and 3).

3. Pore Size Distribution Studies. Figures 6 shows the cumulative intrusion plots for both the CPF slab and the control slab with samples drawn from 0-5 and 5-25 mm depth intervals. Table 1 presents the porosities, the total accessible pore volumes and the threshold diameters for both CPF and control slabs from the mercury intrusion data.

*3.1. Slab ponded from the surface generated by the CPF (CPF slab).* In Figure 6, the steepest portions of the cumulative intrusion plots correspond to the geometrically continuous pore system (capillaries) present in hydrated cement (11). The maximum pore diameter at which the cumulative intrusion curve attains the steepest slope corresponds to the threshold or the neck diameter of the capillary pore system.

In Figure 6, the cumulative intrusion plot for the 0-5 mm depth interval for the CPF slab shows the least total accessible pore volume. This indicates a large reduction in the volume of the geometrically continuous pores for the above depth interval. Table 1 also shows the smallest threshold diameter for the CPF slab at the 0-5 mm depth interval. In contrast, the

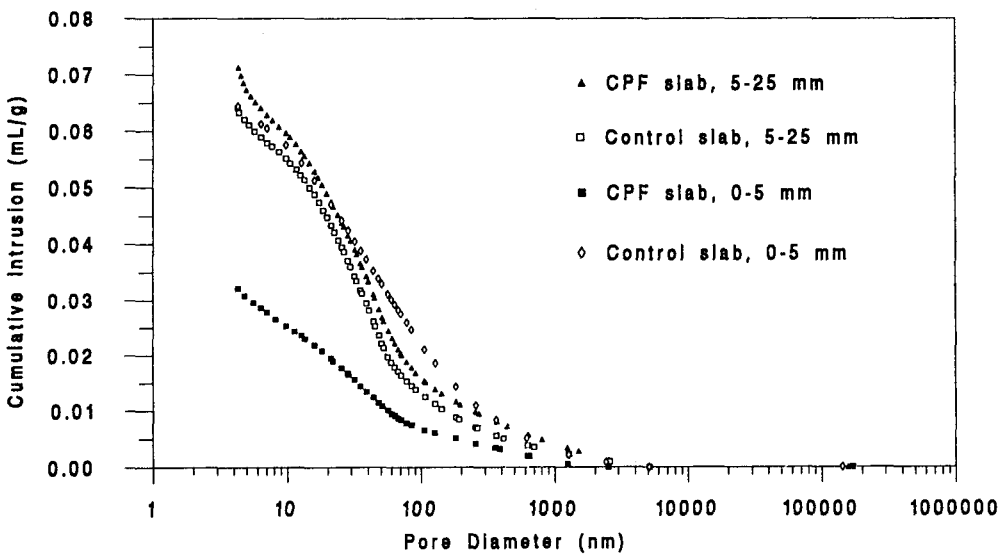


FIG. 6.
Cumulative intrusion plots for the CPF and the control slabs.

TABLE 1

Results from the Mercury Porosimetry Studies

| Slab type | Depth from the ponded surface. mm | Porosity. % | Total accessible pore volume. mL/g-nm | Threshold diameter. nm |
|---|---|---|---|---|
| Slab ponded from the cast face (Control slab) | 0-5<br>5-25 | 13.70<br>12.80 | 0.0644<br>0.0640 | ≈300<br>≈100 |
| Slab ponded from the CPF face (CPF slab) | 0-5<br>5-25 | 6.70<br>13.50 | 0.0321<br>0.0712 | ≈80<br>≈100 |

cumulative intrusion plot for the 5-25 mm depth interval compared to the 0-5 mm depth interval shows more than two fold increase in the total accessible pore volume. Table 1 also shows a similar trend when the porosities for the 0-5 mm (6.70%) and 5-25 mm (13.50%) depth intervals are compared, although the above porosities are not the total porosities of the samples. This is because the maximum pressure limitation of the instrument (30,000 psia) restricts the minimum diameter the mercury can penetrate to around 4 nm (contact angle 117°).

In the following section, those pores with diameters greater than about 100 nm are termed the "large" or the "macro-pores," while those pores below 100 nm are termed the "micro-pores." The macro-pores represent the unfilled void spaces between the cluster of hydration products.

*3.2. Slab ponded from the cast surface (control slab).* In Figure 6, though the cumulative intrusion plots for the 0-5 mm and the 5-25 mm depths intervals show almost identical total accessible pore volumes, the former shows relatively higher pore volumes for the macro-pores. Table 1 shows porosities of 13.70% and 12.80% for the 0-5 mm and the 5-25 mm depth intervals respectively, emphasising that the difference between the above two is insignificant from a practical view point.

The porosimetry results indicate the presence of a relatively denser concrete (minimum macro and micro-pores) at the 0-5 mm depth interval from the CPF for the CPF slab. However, at greater depths beyond 5 mm the CPF appears to be ineffective in generating a similar dense concrete. Furthermore, the 5-25 mm depth intervals of CPF and control slabs have a nearly identical pore structure.

As already pointed out above both the CPF and control slabs carbonated to a nearly similar degree at the 0-5 mm and 5-25 mm depth intervals. Further, the CPF slab showed marginal superiority in resistance to chloride penetration than the control slab at the surface until the 25-45 mm depth interval. However, the mercury porosimetry data showed the presence of a relatively dense concrete for the CPF slab at the 0-5 mm depth interval. Thus, for the CPF slab, the mercury porosimetry data fail to explain the chloride and carbonation (XRD) results.

## Discussion

1. General. For the control slab ponded from the cast face, the presence of CPF at the bottom of the mould should not influence the properties of the concrete at the top cast face. This is due to the fact that the slab is 150 mm thick, and the CPF is reported to be effective upto a maximum depth of 10-30 mm from the CPF mould (1-5,8). Thus, the results presented for the control slab are not influenced by the CPF placed at the bottom of the mould. However, the permeation characteristics of the concrete at the cast surface of the control slab are certainly influenced by the sedimentation effects due to bleeding of the concrete, but the slabs were cast in such a way that bleeding was reduced to a minimum as described at the beginning.

In the present investigation, for mercury porosimetry studies, the coarse aggregates were taken out of the concrete samples as described earlier. This was done in order to eliminate the sample to sample variations arising due to the non-uniform distribution of coarse aggregates in the samples. Otherwise, a concrete sample with higher proportion of coarse aggregate would show a relatively less intruded pore volume, compared to a sample drawn from the same location with a lower proportion of coarse aggregates. Ideally, hydrated cement paste samples are more suitable for mercury porosimetry studies. Further, the removal of coarse aggregates from the concrete might modify the porosity and the pore structure of the original sample. Incidentally, in the present investigation, relative differences in pore structure between the identically prepared samples (mortar) without coarse aggregates are compared. Hence, it is thought that, the method employed provides reliable data for the purpose of relative comparison of the results. Furthermore, the samples thus prepared from cores taken from the same location showed reproducible results. Collepardi et al. (18) have also carried out mercury porosimetry studies on mortar samples obtained by separating coarse aggregates from the concrete samples.

2. Mechanism for CPF Operation. In the present investigation, for both slabs the fabric membrane was fixed at the bottom of the mould. On placing and vibrating the concrete, the fabric membrane as normally expected, drains off the surplus water and the entrapped air from the concrete layer in close contact with the CPF (1-5). As a result of this, voids will be created in a layer of concrete in close contact with the CPF. Due to gravity effect, the cement, aggregates and water from the adjacent concrete layer tend to fill in those voids. Thus, due to the movement of additional cement from the adjacent concrete layer, the concrete layer in close contact with the CPF eventually attains a relatively lower w/c ratio compared to the bulk concrete.

The DTA thermograms confirmed the presence of significant amount of portlandite at the 0-5 mm depth interval of the CPF slab while, portlandite was absent for the control slab at the above depth interval. The above observation is interesting because the 0-5 mm depth interval of both the CPF and control slabs were carbonated to a nearly similar extent. Similarly, for the 5-25 mm depth interval, the CPF slab showed higher amount of portlandite than the control slab despite the fact that both of the slabs were carbonated to a similar extent. The above evidence may suggest the presence of a greater amount of cement at the 0-5 mm and 5-25 mm depth intervals of the CPF slab. The presence of a greater amount of cement at these depth intervals of the CPF slab appears to be due to the movement of additional cement from the adjacent layers as explained earlier. However, for the CPF slab, the 0-5 mm appears to be relatively more rich in cement than the 5-25 mm depth interval. This is confirmed by the presence of slightly greater amount of portlandite at the 0-5 mm than the 5-25

mm depth interval in spite of the fact that the former was carbonated to a relatively higher extent.

3. Chloride Penetration and Carbonation. The above discussion suggests the movement of additional cement into the concrete layer in contact with the CPF from the adjacent layers. However, it is not clear how far the increased cement content at the 0-5 mm and 5-25 mm depth intervals of the CPF slab has reduced the local w/c ratio of the concrete from the w/c ratio of the bulk concrete. Research reported by the present authors (19) has clearly demonstrated the penetrability of chlorides in substantial amounts until the 25-45 mm depth interval even through concrete of 0.45 w/c ratio on long-term exposure (70 cycles of wetting and drying). Thus, long-term resistance to chloride penetration in concrete structural elements cast with CPF is achievable provided the CPF generates a dense concrete skin of w/c ratio anything below 0.45.

In the present investigation the atmospheric carbonation of slabs is not expected to occur during the 7 day wetting period of the 10 day cycle. This is due to the unfavourable RH, as air permeability of concrete decreases markedly above 80% RH (20), and the maximum carbonation is at 50% RH (21). The atmospheric carbonation may start during the 3 day drying period of the 10 day cycle at some rate, but it is considered that it will be at a very slow rate and much below the optimum rate. This is due to the limited drying of capillary pores which enhances the flux of $CO_2$ through the concrete. Thus, the severe carbonation of the slabs is believed to have taken place during the one and half years time gap between the 50 and 70 exposure cycles, and also during the two and half years time gap after the completion of the 70 exposure cycles.

Recalling from the section on experimental work, it is emphasized that the pore structure study was carried out by taking fresh cores from both slabs on completion of the exposure regime. Thus, it is natural that the pore structures presented above have been modified by the penetrating chloride ions and the carbonation products. As already pointed out earlier, at the 0-5 mm depth interval, the CPF slab showed significant reduction in the number of macro pores (>about 100 nm in diameter) compared to the control slab. According to Powers (22), the macro pores provide numerous nucleation sites for the atmospheric carbonation attack. In contrast, atmospheric carbonation attack is inhibited in the micro pores due to inadequate nucleation sites. This is due to the fact that the macro pores have a large internal pore wall surface area compared to the micro pores. The preferential precipitation of $CaCO_3$ in the macro pores as explained earlier modifies the pore structure. It is reported that due to the atmospheric carbonation of concrete the number of pores in the range of 20-1000 nm in diameter is reduced (23). Further, the products due to atmospheric carbonation of concrete such as calcite, aragonite and vaterite are voluminous. Thus, conversion of each gram mole of portlandite into $CaCO_3$ results in an increase of 11.8% in volume (15). The diffusing chloride ions derived from NaCl are also known to decrease the number of pores around 80 nm in diameter (24).

The above modifications due to the atmospheric carbonation and penetrating chlorides are superimposed on the pore structure generated at the cast and the CPF faces due to hydration. Thus, for the CPF slab, at the 0-5 mm depth interval, the chlorides and atmospheric carbonation products further decrease the number of macro pores from the relatively dense pore structure generated by the CPF. The relatively lesser number of micro pores for the CPF slab at the 0-5 mm depth interval is believed to be mainly due to the effect of CPF. On the other hand, for the control slab, both chlorides and carbonation products decrease the macro pore volumes of the relatively coarse pore structure generated at the cast face. The rise in the

number of pores less than around 4 nm diameter due to the possible partial blocking of the macro pores by chlorides and carbonation products cannot be seen due to the pressure limitation (maximum 30,000 psia) of the porosimeter. It is important to note that both slabs were cured and exposed to identical exposure regimes, hence the observed differences in the pore structure are not influenced by the differences in degrees of hydration. Thus, the pore structure presented here for CPF slab is not solely due to the presence of CPF at the bottom of the mould; it is a modified structure due to penetrating chlorides and carbonation products.

The XRD and DTA results showed an almost similar degree of carbonation for both CPF and control slabs at the surface. Also, the CPF slab showed a marginal superiority against chloride penetration at the surface compared to the control slab. One is thus lead to believe that, the pore structure and permeability of the concrete at the ponded surface in both the slabs after 28 day curing were not very different from the view point of resistance to chloride and carbonation attack. Thus, it appears that, the CPF employed at the bottom of the mould decreased marginally the w/c ratio of the concrete adjacent to it from that for the bulk concrete. The concrete thus generated adjacent to the CPF was not dense enough to effectively control the transportation of chlorides and atmospheric $CO_2$ through it. This suggests that the CPF is not fully effective in its intended purpose of generating a permanent and long-lasting dense impermeable concrete layer adjacent to it for concrete of 0.60 w/c ratio.

## Conclusions

The following conclusions are derived from the present investigation.

1. The CPF employed at the bottom of the mould decreases the w/c ratio of the concrete adjacent to it marginally compared to the w/c ratio of the bulk concrete. Thus, the CPF is not fully effective in its intended purpose of generating a long-lasting dense impermeable concrete layer adjacent to it when the w/c ratio of the concrete mix was 0.60.
2. Due to the CPF not generating a dense impermeable concrete, the CPF slab, exposed from the face generated by the CPF, carbonated to an almost similar extent (XRD and DTA) as that of the control slab exposed from the cast face.
3. Also, due to the failure of CPF in generating a dense impermeable concrete, the CPF slab, ponded from the surface generated by the CPF showed almost similar amount of chlorides and their depths of penetration as that of the control slab exposed from the cast face, although the CPF slab was marginally superior in chloride penetration resistance at the surface.
4. Severe atmospheric carbonation and chloride ion penetration through concrete results in substantial modification to the original pore structure.

## Acknowledgement

The authors are grateful to Prof. J.H. Sharp, Head, Engineering Materials Department for providing experimental facilities.

## References

1. K. Tanaka and H. Ikeda, IABSE Symposium Report, 55, 345(1988).
2. Y. Kasai, M. Nagand, K. Sato and K. Suga, Transaction of the Japan Concrete Institute, 10, 59(1988).

3. Y. Kasai, K. Sato and M. Nagana, Cement Association of Japan, Technical Session 43rd Review Report, 298(1988).
4. J. Annie Peter and N. Chithranjan, The Indian Concrete Journal, 69, 215 (1995).
5. W.F. Price and S.J. Widdows, Magazine of Concrete Research, 43, 93 (1991).
6. ASTM 4491-85, Standard Test Method for Water Permeability of Geotextiles by Permittivity, 04.08, 693 (1988).
7. ASTM D737-75, Standard Test Methods for Air Permeability of Textiles Fabrics, 07.01, 123 (1988).
8. S.A. Reddi, The Indian Concrete Journal, 66, 31 (1992).
9. BS 1881:Part 124, Determination of Chloride Contents, 17 (1988)
10. L. Konecny and S.J. Naqvi, Cem. Concr. Res, 23, 1223 (1993).
11. D.N. Winslow and S. Diamond, Journal of Materials, 5, 564 (1964).
12. Jaw-Chang Laiw, Ph.D. thesis, University of Sheffield (1992).
13. Highway Research Board, Guide to Compounds of Interest in Cement and Concrete Research, Highway Research Board Special Report no.127, 28 (1972).
14. J.E. Ash, M.G. Hill, J.I Longford and M.Mellas, Cem. Concr. Res, 23, 399 (1995).
15. D.R. Moorehead, Cem. Concr. Res., 16, 700 (1986).
16. Z. Sauman, Cem. Concr. Res., 1, 645 (1971)
17. V. Pavlik, Cem. Concr. Res, 24, 1495 (1994).
18. M. Collepardi, A. Marcialis and R. Turriziani, Journal of American Ceramic Research Society, 55, 534 (1972).
19. A.K. Suryavanshi and R.N. Swamy, Cem. Concr. Res, 25, 729 (1996).
20. L.J. Parrot, Report of RILEM Technical Committee 116-PCW, RILEM, 1990.
21. O.E. Gjorv, Proc. of EVALMAT, 565 (1989).
22. T.C. Powers, Journal of Portland Cement Association, Research Development Laboratory, 4, 40 (1968).
23. P.J. Dewaele, E.J. Reardon and R. Dayal, Cem. Concr. Res., 21, 441 (1991).
24. H.G. Midgley and J.M. Illston, Cem. Concr. Res., 14, 546 (1984).